# The Residual Strain in a Reservoir Ice Cover: Field Investigations, Causes, and Its Role in Estimating Ice Stress

Wenfeng Huang[1], Zhijun Li[2], Matti Leppäranta[3], Hongwei Han[4], Ni Wang[5]

[1] Lecturer, Key Laboratory of Subsurface Hydrology and Ecological Effects in Arid Region of the Ministry of Education, School of Environmental Science and Engineering, Chang'an University, Xi'an 710054, China (Corresponding author). E-mail: huangwenfeng@chd.edu.cn

[2] Professor, State Key Laboratory of Coastal and Offshore Engineering, Dalian University of Technology, Dalian 116024, China. E-mail: lizhijun@dlut.edu.cn

[3] Professor, Department of Physics, University of Helsinki, Helsinki FI-00014, Finland. E-mail: matti.lepparanta@helsinki.fi

[4] Lecturer, School of Water Conservancy and Civil Engineering, Northeast Agricultural University, Harbin 150030, China. E-mail: hhw777@sina.com

[5] Lecturer, Key Laboratory of Subsurface Hydrology and Ecological Effects in Arid Region of the Ministry of Education, School of Environmental Science and Engineering, Chang'an University, Xi'an 710054, China (Corresponding author). E-mail: 282864934@qq.com

**Abstract:** Ice strain dominates the ice thrust and dynamics on reservoir dams and retaining structures. An exclusively designed laser range finder was deployed to measure the surface ice displacements along six directions at a reservoir in northeastern China. The incompletely confined boundary (ice-boundary bonding), ice cracks development, water level fluctuations, parallel crack dynamics, and ice creep allow the surface ice to move rather than keep still in response to thermal deformation/pressure, and thus cause the ice strain deviates from thermal strain. Consequently, a residual strain was introduced and calculated from the recorded displacements. Observations showed that the residual strains were anisotropic and showed diurnal patterns following the air/ice temperature. A scale-dependence of crack development was observed and causes potential scale-effects to residual strains. The real ice strain consists of thermal strain and residual strain. The proportion of the latter increased as time went by. A modified constitutive law accommodating the residual strains was developed to evaluate the impacts of the residual strains and to estimate the surface ice stresses. Modeling results underlined the role of the residual strain in determining both the principal stress and the stress perpendicular to and parallel with the dam face. The residual strain is probably the reason why the observed ice stress is always much lower than the single thermal stress.

**Keywords:** thermal strain; residual strain; constitutive law; static ice loads; reservoir ice

## Introduction

Although dams have been built and operated for a long time in northern climate, the forces exerted by ice on them are still not well understood. These loads must be taken into consideration in design of ice-infested hydraulic structures and engineering (Cox 1984; Bouaanani et al. 2004), but there is still not enough information available to predict these loads with a satisfactory confidence for engineers (Comfort et al. 2000a,b; Gebre et al. 2013). Horizontal ice forces on structures are usually divided into two broad categories: static forces produced by a structure constraining the thermal expansion of an ice cover in horizontal plane, and dynamic forces created by the interaction of moving ice cover with a fixed/moving structure.

Ice pressure is an important stress value to be measured in determining the static ice loads (Comfort et al. 2003; Taras et al. 2009). Previous findings have revealed that the ice pressure in reservoirs can arise from various processes that can act alone or in combination. Among these processes, one can identify thermal forces (Cox 1984; Ko et al. 1994; Comfort et al. 2003), forces associated with changes in water level (Stander 2006; Taras et al. 2009) and wind forces (Prinsenberg et al. 1997). Furthermore, in situ data and theoretical analyses also indicate that the magnitude of thermal ice load is affected by the snow/slush cover, ice thickness, shoreline confinement, reservoir shape, and relative stiffness of various hydraulic structures (Boulton and Jones 1979; Comfort et al. 2000b,c; Arunachalam 2005; Petrich et al. 2015). Most of theoretical predictions of the maximum ice thrust are based on a simple in-plane compressive model of fragmented ice floes with respect to buckling/bending and hinging effects (Carter et al. 1998), which derives an upper bound for ice thrust. Instead, some empirical functions have been reported to show encouraging ability to estimate the thermal loads of an ice cover based on the elastic and viscous behavior of ice (Xu 1986; Bergdahl 1978; Cox 1984; Fransson 1988). Current models consistently overestimate the ice stress, but the reasons for this overestimation are still not well understood (Azarnejad and Hrudey 1998; Comfort et al 2003).

Conventionally, field measurements of ice thrust/load rely on various stress sensors refrozen between ice and dam face, or within ice. However, occasional detachments and poor bonds between ice and sensors contaminate the data quality. Therefore, ice deformation or strain measurement provides an indirect way to determine the ice stress in a reservoir (Morse et al. 2009, 2011). Additionally, the ice push and sudden displacement due to the release of cumulated ice stress/strain can damage the dam revetments, ice-infested hydro-structures, and even buildings on the shore (Comfort and Liddiard 2006). Hence, the determination of the ice strains and their accumulation is of great importance in understanding and modeling the ice thrust in lakes and reservoirs. Nevertheless, ice displacement and strain have not been well quantified especially in field scale.

A field campaign was conducted between February 24 and March 26 in 2011 to monitor the surface ice displacement in Hongqipao Reservoir, northeastern China. This paper presents the in situ investigations and results, aiming at quantifying the residual strain within the ice cover and relating it to environmental conditions to better understand the mechanism of ice thrust. A new constitutive model was then developed to estimate the ice stress and to evaluate the effects of environmental conditions besides the air/ice temperature.

## Field Investigations

Hongqipao Reservoir (46°36'N, 125°16'E) is located in Daqing, Heilongjiang Province, northeastern China. The reservoir area is 35 $km^2$ with a storage capacity of $1.16\times10^8$ $m^3$, bound at the western, southern and eastern sides by concrete panel-paved earth-filled dams. The dams are totally 24.5 km long. Ice season usually begins in later October or early November when the air temperature descends below 0°C, and ends in middle or late April. Ice thickness can be up to 1.20 m in March when the air temperature is still below the freezing point of freshwater (Fig. 1). Over the whole ice season, water replenishing is ceased, although one intake works for water supply. The water level fell by only 0.05 m from 147.18 m to 147.13 m during the two weeks of measurement, and the current velocity under ice was assumed to be negligible (Fig. 2).

An automatic laser range finder (LRF) was developed exclusively to measure the distance (i.e. displacements of surface ice) along any direction. LRF consists mainly of two parts: a high-resolution laser range finder (Leica Disto D3A) and a steerable automatically-rotating base. The ranger finder has an accuracy of ± 1 mm (with a reading resolution of 0.1 mm) within the measuring range of 0.05 – 200 m. The rotating base has a direction accuracy of ± 1°. These two parts were modulated and connected to a laptop, which functioned as a controller and data logger. The field design and instrumentation is shown in Fig. 3. Six reflectors (Points P1 ~ P6) were fixed and refrozen quickly into the ice cover around the LRF (Point O) to reflect the laser transmitted by the LRF for distance recordings. All reflectors were spaced 60° apart from one another, with P1 pointing to the geographic north. The lengths of the lines OP1, OP2, …, OP6 were 4.9 m, 7.9 m, 10.8 m, 13.9 m, 16.9 m and 19.9 m, respectively. The LRF was at about 40 m distance from the dam face.

In order to avoid the contamination in the displacement data induced by wind force and surface melting of snow/ice, the LRF was fastened to a platform through 4 screws. The platform had three 90 cm-long wooden legs (like a tripod), all of which were inserted into the ice sheet to a depth of approximately 50~60 cm (similar to the technology deployed in polar ice observations by Polashenski et al. (2012)). The platform was carefully leveled using a bubble level before its legs were refrozen fasten into the ice holes. Every reflector had also a 90 cm-long wooden leg, which was inserted into the ice cover to a similar depth (50~60 cm). Therefore, the maximum heights of the LRF and reflectors were lower than 40 cm beyond the ice surface, reducing the wind effect. Furthermore, all surfaces and legs of the reflectors and LRF platform were colored white to avoid radiative absorption that might induce internal melting at the wood-ice interfaces.

A meteorological station was established 30 m away from the LRF to measure and record the net radiation, air temperature, and wind speed and direction once a minute. A thermistor chain was placed into a drill hole, and refrozen into the ice cover to measure the ice/water temperature at 2-122 cm below the ice surface at 5-20 cm vertical spacing (at 2 cm, 7 cm, 12 cm, 17 cm, 22 cm, 27 cm, 32 cm, 42 cm, 52 cm, 62 cm, 82 cm, 92 cm, 102 cm, and 122 cm). The resolution was 0.1 °C for temperature, 1 W/$m^2$ for irradiance, 0.1 m/s for wind speed, and 1° for wind direction. An ultrasound sonar with 2-mm accuracy was placed 50 cm below the ice bottom to record the ice thickness at every half hour. The initial ice thickness was 90 cm when the ice was instrumented on February 24. Meanwhile, ice thickness was also measured manually every two or three days using an ice auger. All measurements were ended on March 28 when the piles tilted.

However, due to power and machinery failure, surface ice displacement datasets were obtained discontinuously before March 4. And the data recorded after March 20 was false since the reflector stands started to become loose due to ice melt. Therefore, a 16-day period of good data was obtained and is further analyzed here.

## Constitutive Laws

### *Current Constitutive Laws*

In order to illustrate thermal ice displacements directly, we assume that the ice cover (or the surface layer) is isothermal and homogeneous all time, and that the ice temperature changes instantaneously. Fig. 4 illustrates the thermally induced ice deformation under three kinds of constraint boundaries (free, fixed, and incompletely confined ends) when the ice temperature changes. The points O and $P_i$ denote the LRF and an arbitrary reflector in Fig. 3.

Under the free boundary condition, with an increment in ice temperature ($\Delta T$, °C), the length of

$OP_i$ expands from its initial $L_0$ to $L_T$,

$$L_T = L_0(1+\alpha\Delta T), \quad (1)$$

where $\alpha$ is the thermal expansion coefficient of freshwater ice ($5.0\times10^{-5}$°C$^{-1}$). There is no stress within the ice cover.

Under the fixed boundary (i.e. completely confined), points O and $P_i$ never move with changes in temperature for an intact ice cover, and the thermal strain $\varepsilon_T$ and stress $\sigma_T$ (Pa) can be expressed as

$$\varepsilon_T = \frac{L_T - L_0}{L_0} = \alpha\Delta T, \quad (2)$$

$$\sigma_T = E_i\varepsilon_T = \alpha E_i \Delta T, \quad (3)$$

where $E_i$ (Pa) denotes the elastic modulus assuming the ice is an elastic medium. Usually, freshwater ice is regarded as an elastic-viscous medium and modeled using a Maxwell unit (a spring, which represents instantaneous elastic deformation, in series with a nonlinear dashpot based on a power law creep which models the non-recoverable viscous deformation) (Bergdahl 1978; Azarnejad and Hrudey 1998; Petrich et al. 2015). Thermal ice pressure can be formulated as

$$\frac{d\sigma_i'}{dt} = E_i\left[\frac{d\varepsilon_i}{dt} - KD\left(\frac{\sigma_i}{\sigma_0}\right)^n\right], \quad (4)$$

where $t$ is time (s), $D$ is the temperature-dependent viscous creep rate ($m^2/s$), $K$ ($m^{-2}$) and $n$ are viscous rheology parameters, $\sigma_0$ is a reference stress (Pa), and the subscript $i$ stands for the ice. The first and second term in the square brackets represent the instantaneous elastic strain and time-dependent viscous strain, respectively.

Taking into consideration the material nature of freshwater ice, some complicated physically-based models primarily consisting of a Maxwell unit in series with a Kelvin-Voigt unit (i.e. a spring parallel to a nonlinear dashpot, representing the delayed elastic deformation) or other combinations of several Maxwell and/or Kelvin-Voigt units have been proposed (Yamaoka et al. 1988; Ivchenko 1990). However, comparisons with analytical results and field tests indicated that the models including only a Maxwell unit (Eq. (4)) show a better prediction and require less computing consumption (Azarnejad and Hrudey 1998; Petrich et al. 2015).

The ice strain rate is currently considered to be equal to the thermal strain rate (Bergdahl 1978; Cox 1984; Timco et al. 1996; Petrich et al. 2015)

$$\frac{d\varepsilon_i}{dt} = \frac{d\varepsilon_T}{dt} = \alpha\frac{dT}{dt}. \quad (5)$$

Thus, Eq. (4) is transformed into

$$\frac{d\sigma_i'}{dt} = E_i\left[\alpha\frac{dT}{dt} - KD\left(\frac{\sigma_i}{\sigma_0}\right)^n\right]. \quad (6)$$

***A New Constitutive Law***

Under incompletely confined boundary (e.g. elastic restraint), which is representative of natural static lake and reservoir ice covers, especially for a tilted dam, the ice cover also expands (thick black dotted lines in Fig. 4) but not as much as the free boundary, i.e., the length $L_0$ grows to $L_B$ with an increase in ice temperature. Therefore, the real ice strain $\varepsilon_i$ is

$$\varepsilon_i = \varepsilon_T - \varepsilon_R = \alpha\Delta T - \frac{L_B - L_0}{L_0}, \quad (7)$$

where $L_0$ and $L_B$ are the original distance and the distance after a temperature change, respectively, and the residual strain $\varepsilon_R = \frac{L_B - L_0}{L_0}$ (8)

was determined from the displacements of the LRF and reflectors.

Eq. (6) is thus transformed into

$$\frac{d\sigma_i}{dt} = E_i\left[\frac{d}{dt}(\alpha T - \varepsilon_R) - KD\left(\frac{\sigma_i}{\sigma_0}\right)^n\right]. \quad (9)$$

This represents a modified Maxwell constitutive model with linear elastic and nonlinear viscous parts. The residual strain would cause the ice stress to deviate from those created by the thermal strain alone.

***What Is the Residual Strain $\varepsilon_R$?***

The residual strain $\varepsilon_R$ is defined as Eq. (8), and is introduced to the most common constitutive law (Eq. (6)), representing the responses of the surroundings to changes in ice temperature (i.e.

thermal stresses), for instance, the ice edge dynamics on the tilt dam face and natural slopes and along the parallel cracks, the development of surface cracks, and the water level fluctuations.

If it is assumed that the intact ice cover (without cracks and ridges) is fixed completely to the reservoir boundaries (dams and land slopes), the reflectors in Fig. 3 and 4 should not move in response to a temperature change, and the ice strain consists solely of thermal strain $\varepsilon_T$ (Eq. (2)). Actually, physical processes in response to the thermal loads drive the piles to move back and forth, thus producing the residual strain $\varepsilon_R$. For instance, the ice edges indeed move forwards and backwards restrainedly (adhesive sliding) on the dam faces or slopes due to the thermal expansion and contraction of ice cover (Fig. 5), somehow releasing the thermal strains (Morse et al. 2009, 2011). Tensile stresses due to ice contraction or shear stresses give rise to intensive cracks and fissures especially within the surface layer of the ice cover (Fig. 5a). With a rise in ice temperature (Fig. 5b), old cracks close, and the target pile moves from $P_i(a)$ to $P_i(b)$ due to thermal expansion. With a following fall in temperature (Fig. 5c), the ice cover contracts, the closed cracks open, and new cracks occur for the ice cannot hold high tension because of its low tensile strength. Therefore, the target pile $P_i(b)$ usually does not return to its original place $P_i(a)$, but to $P_i(c)$, causing an accumulated displacement. The opening and closing of the cracks also absorb thermal strains. The reservoir shape can cause a spatial variability of thermal strains. Moreover, the ice cover bending and buckling due to the rise/fall of water stage inevitably creates additional surface strains (Stander 2006). The time series of the distance $P_0P_i$ were observed and recorded by the LRF. We are currently not able to partition the contributions of all above processes, but they are embodied jointly in the residual strain $\varepsilon_R$. In other words, the ice strain should consist of thermal strain $\varepsilon_T$ and residual strain $\varepsilon_R$ (Eq. (7)).

## Data Processing

Dry and wetted cracks develop extensively over the reservoir ice cover and have a significant impact on the static ice strain/stress and loads (Azarnejad and Hrudey 1998), especially the prolonged parallel and circumferential cracks breaking the ice cover (Carter et al. 1998; Comfort et al. 2003). In order to investigate the general features of surface cracks, 138 individual snapshots of ice cracks and an image mosaic covering a 5 m × 50 m area (Jia 2012) were reanalyzed using image processing method similar to Huang et al. (2016) to explore the crack density (crack area per unit ice surface area) and its spatial variation. Within differing spatial scales from 2 m to 24 m, the averaged crack densities and their standard deviation (STD) were calculated.

To assess the internal consistency of displacement data, frequency analysis was applied to the raw datasets. Power spectrums for directional displacements (Fig. 6) indicated evidently that all directional displacements except P1 have the same patterns of frequency distribution to the surface ice temperature and were in phase with each other. There were two main periods: one day and approximately 5-8 days, which correspond to the diurnal cycle of temperature and durations of cold/warm spells, respectively. However, P1 displacement did not show any obvious main frequency/period.

Prior to displacement data processing, the atmospheric and earth curvature corrections were estimated to be approximately 2 ppm (or 2 mm/km) under typical weather conditions. The calculated distance corrections were actually negligible since the present measuring distances were not longer than 20 m. Although careful installation technologies were used to prevent the LRF and reflectors movement induced by surface melting and the exposure heights of them were set quite small, strong winds induced LRF and reflector vibrations as well as the LRF accuracy introduced approximately 1~2 mm fluctuations in observed displacements. Therefore, a filtering process (3-hours moving average) was applied to remove these environmental distortions. The smoothed displacement datasets were used for further calculations in present study.

A seven-parameter similarity (Helmert) transformation is typically used to compensate the impacts of LRF movement (Prat et al. 2012). This could not be done because we did not design reference targets that did not move. However, in present work the LRF was positioned between the reflector pairs of P1-P4, P2-P5, and P3-P6, namely, LRF was in the straight lines of P1-P4, P2-P5, and P3-P6. Therefore, the integral residual strains along these three lines can be calculated as:

$$\varepsilon_{\mathrm{R14}} = \frac{\Delta L_1 + \Delta L_4}{L_1 + L_4} \approx \frac{\Delta L_4}{L_4}, \quad (10)$$

$$\varepsilon_{\mathrm{R25}} = \frac{\Delta L_2 + \Delta L_5}{L_2 + L_5} \left(\approx \frac{\Delta L_5}{L_5}\right), \quad (11)$$

$$\varepsilon_{R36} = \frac{\Delta L_3 + \Delta L_6}{L_3 + L_6}, \quad (12)$$

**Field Code Changed**

where, $\Delta L_i$ is the distance change of Po-Pi, and $L_i$ is the original distance of Po-Pi. Note that the residual strain of line P1-P4 ($\varepsilon_{R14}$) is calculated using only data of Po-P4 since P1 is abnormal (discussed later). In this way we can significantly take away the effect of possible LRF movement on residual strains. As reference, the individual residual strains of every reflector were also calculated.

In order to calculate the static stress (load) of surface ice using Eq. (9), a thin surface layer is assumed to be detached from the ice cover for modeling purpose (similar to Bergdahl (1978), Morse et al. (2009), and Petrich et al. (2015)). The averaged value of air and 2-cm depth temperature is assumed to be the representative temperature of the thin surface layer.

## Results and Analysis

### ***Ice Thickness and Temperature***

When the field campaign was established, there was a discontinuous snow cover due to uneven accumulation by winds. The thickness of snow 2 m around Point O was up to 30 cm, while only about 3 cm thick or less snow was distributed at other points. No new snow fell through the entire instrumented period. Snow cover melted away on March 15 when air temperature rose above 0 °C. Much melt water accumulated in depressions of ice surface.

The ice cover grew or melted quite slowly, and in the period of the experiment the ice thickness remained within 93 ± 2 cm. The ice consisted predominantly of coarse columnar-grained ice (S2 type) with the topmost 1-2 cm of fine granular snow ice. The ice temperature above 35 cm depth followed the variations of daily air temperature cycle with damping and time lag increasing with depth (Fig. 7). Although the diurnal variations in ice temperature below 35 cm depth were negligible, there was a gradual increase due to increasing mean air temperature, enhancing solar radiation, and cold/warm spells. The ice temperature at 2 cm depth was much closer to air temperature during the last few days due to surface melting and ablation.

After a few stable diurnal cycles with daily mean value of -9 °C in phase (a), the representative ice temperature increased with diurnal oscillations to a peak (~ -1.0°C) in phase (b), decreased to -10.0°C in phase (c), and then rose sharply to approximately 0°C within two days (phase (d)). Through the observation, northern winds prevailed, and the mean wind speed (2 m above the ice surface) was 3.5 m/s.

### ***The Observed Residual Strain $\varepsilon_R$***

The observed residual strain $\varepsilon_R$ was generally lower than thermal strain $\varepsilon_T$ for an arbitrary temperature increment (Fig. 8). Since their initial positions, surface ice mostly contracted along the directions of P1, P2, and P4, and expanded along P3, P5, P6, P25 and P36 directions. Although the ice cover was constrained by the firm boundaries, along all directions (P1 ~ P6), the ice showed a diurnal cycle of expansion and contraction in response to the daily evolution of air/surface ice temperature, and also a seasonal variability following the cold/warm spells (also in Fig. 6). Directional displacements/residual strains had a rough phase (time) lag of 0.5−2 h compared to ice temperature/thermal strain. But there are generally differences between expansions and contractions within the same day (Fig. 8), leading to growing accumulated permanent displacements. In addition, within an individual phase of temperature rise/fall, the ice displacement was able to shift from expansion to contraction, or conversely, such as P1, P2, and P4 in phase (c).

Obviously, the P1 displacement differed significantly in magnitude and even pattern from others. And the P2 displacement gave little physical senses since it roughly contracted but P6 (in the same line) expanded. The scale variability of the spatial distribution of surface cracks is likely one process accounting for it. For a static ice cover, flaws and cracks exist densely over the ice surface due to compressive, tensile, and shear stresses caused by water level variations, winds, as well as temperature changes. Crack image processing (Fig. 9) indicated that the averaged crack densities beyond 2 m scale are coincidently 4.6%~4.9% and show little scale dependence, but their STD values show a significant scale-dependence, namely, STD decrease from 2.2% to 0.9% as the spatial scale increases from 2m to 12m, and remain around 0.9% when the scale grows beyond 12 m. Therefore, the displacement can be impacted potentially by the spatial variability of crack development if the length between reflectors and LRF is less than 12 m (such as P1, P2, and P3).

On the other hand, the seasonal and diurnal amplitudes of P2 displacement were approximately 1-2 mm and 2-3 mm, respectively. These values were very close to the LRF measuring accuracy (±1 mm), indicating the LRF could not detect effectively changes in P2 displacement. This might also lead to a distinct displacement regime in P1. Consequently, the displacement datasets from P3, P4, P5, P6, P25, and P36 are favorably representative of the entire ice cover, and were used to calculate the ice strain/stress.

***Surface Ice Strain $\varepsilon_i$***

Eq. (7) gives the surface ice strain taking into consideration the observed residual strain $\varepsilon_R$. Fig. 10 presents the strains perpendicular to and parallel with the nearby dam and the first principal strain with its direction derived from lines P4, P25, and P36. All directional and principal strains showed significant discrepancies from the thermal strains, especially after the warm spell (phase (b)), though they show similar temporal trends. The principal strain direction gradually turned to north (roughly towards to the reservoir center) despite of its early significant fluctuation. This is attributed to the boundary shape and spatial differences in ice temperature changes due to uneven snow cover (Prat et al. 2012; Petrich et al. 2015).

The normal strains close to the dam were consistently lower than the thermal and principal strains while the parallel strains were always close to or slightly larger than the thermal strains. As the residual strains accumulated with time, the discrepancies between thermal and directional (also normal and parallel) strains also increased gradually, perhaps due to the piling up and climbing of ice onto the dam face, crack formation and evolution, and ice creep (Fig. 5).

Removing the abnormal P1 and P2 displacements, there were directional strains of P3, P4, P5, P6, P25, and P36. They were combined to create 9 equiangular strain-gauge triangles including 2-3-4, 2-4-6, and 2-4-36. The values and directions of the first principle strains were calculated for each triangle (Fig. 11). Results of triangles 4-25-36, 4-5-36, 4-25-3, 4-25-6, 4-5-6, and 4-5-3, agree each other quite well with respect to principle strain and its direction. Triangles 2-3-4, 2-4-6, and 2-4-6, also match each other very well, but they deviate much from triangle 4-25-36 since March 10th, especially with respect to directions (Fig. 11c). To take away noise, the daily averages of principle directions were calculated for all triangles in Fig. 11d, where they tell overall the same story, especially for triangles 4-25-36, 4-5-36, 4-25-3, 4-25-6, 4-5-6, and 4-5-3.

Generally, triangles 2-3-4, 2-4-6, and 2-4-6 match not very well triangles 4-25-36, 4-5-36, 4-25-3, 4-25-6, 4-5-6, and 4-5-3. The reason is that the LRF cannot resolve precisely the small displacements of P2. It also indicates that the surveying distance of present LRF should be longer than some 10 m (based on P3) in order to achieve a good precision in ice surface deformation surveying. Consequently, the results of triangle 4-25-36 were used to estimate the ice stress hereafter for the sake of precision and convenience.

***Estimate of Surface Ice Stress***

Taking into consideration the observed residual strains $\varepsilon_B$, a modified constitutive model was developed to estimate the ice stresses (Eq. (9)). The values of all involved parameters and coefficients are assigned in Table 1. The principal, normal and parallel stresses showed similar trends with the ice temperatures and thermal stresses (Fig. 11), but the principal stresses were quite close to the thermal stresses except during the temperature surge (phase (d)). The normal stresses were always lower than the thermal ones, especially they were lower by more than 250 kPa (~35%) during the warm spells, indicating the residual strains created a considerable relief to the thermal loads normal to the dam face. This argued that a significant error can be produced by the ignorance of environmental responses to thermal loads; for instance, ignorance of ice dynamics on the dam face, the development and evolution of cracks, the changes in water level (Stander 2006; Taras et al. 2009), and wind stresses (Prinsenberg et al. 1997). The stresses parallel with the nearest dam face kept even equal to the thermal stresses except during the temperature phase (b), when the parallel stresses became larger than thermal ones. The parallel stresses were generally larger than normal ones over the observing period. The lateral confinement ratio of parallel to normal stress had a roughly increasing temporal trend from 0.5 to 1.7 with a median of 1.08 and a mean of 1.35. The lateral confinement degree is believed to be controlled predominantly by the boundary shape, the spot location, the spatial variability of ice temperature change, as well as the water level variation if any (Morse et al. 2011; Prat et al. 2012; Petrich et al. 2015).

***Strain Rates***

Conventionally, the maximum ice load is believed to occur when the ice cover fails on the dam face in compression. The compressive strength of freshwater ice determines the maximum load. Freshwater ice is a viscoelastic medium with a strain rate dependent compressive strength. For strain rate lower than $10^{-4}$/s, ice shows ductile behavior, and its strength increases in way of a power law function against an increased strain rate. For the strain rate larger than $10^{-3}$/s, ice is brittle, and its strength decreases rapidly with increasing strain rate. Within the ductile-brittle transition zone ($10^{-4}$—$10^{-3}$/s), the peak strength is reached, approximately 3 MPa at -10°C (Zhang et al. 2012). The time derivatives of Eq. (2), (8) and (7) provide the strain rates of thermal strain, residual strain, and surface ice strain, respectively (Fig. 12). The strain rates of the thermal strain and residual strain are of similar magnitude ($10^{-9}$—$10^{-7}$/s), which is consistent with the field observations by Morse et al (2009). But the integrated strain rate has a wider range of $10^{-11}$—$10^{-6}$/s magnitude. At this range, the compressive strength is lower than ~1.4 MPa (-10°C), and the elastic modulus is believed to be lower than 1.5 GPa (Han et al. 2016). This is also the reason why the stress borne by the dam face should not surpass 1.4 MPa (e.g. Fig. 11, Morse et al. 2009; Taras et al. 2009) and why the elastic modulus used in Table 1 is much lower than the values (4—9 GPa) usually used before.

## Discussion

***The Capability of LRF and Uncertainties***

The surface ice displacements were measured in a plain reservoir of northeastern China using a laser ranging device. This study gave an opportunity to directly quantify the deviations of real ice strain to thermal strain. The deployed LRF provided excellent, site-scale, real-time measurements of surface ice displacements. Relatively, conventional contact strain and stress sensors can cause significant systematic errors when the expansion coefficient of the sensor material is close to that of ice, while LRF is free of this problem. LRF can measure the deformation of adequate length to cover the universal impacts of field-scale crack development (e.g. scale >12 m in the studied reservoir), which is almost impossible to be reproduced in cold laboratories. However, the ability of the present device is also limited by some uncertainties. According to the present measurements, the LRF with an accuracy of 1 mm is not able to effectively detect the diurnal changes in P1 and P2 displacement, namely, its accuracy predetermines a minimum effective measuring distance, of which the deformation can be effectively sensed. For instance, the minimum distance should be larger than ~ 10 m in Hongqipao Reservoir. Within the given measuring range of LRF, the longer the measuring distance is, the more precisely the LRF works. But the atmospheric correction should be done for observed distance data (Prat et al. 2012).

Another uncertainty in LRF measurements is induced by the wind-induced vibration of reflectors. Although we were intended to reduce the exposure heights of LRF and reflectors, the wind-induced distortions (often at high frequency) bring some fluctuations to the displacement datasets. These fluctuations are more significant in P2 and P3 than P4-P6, but don't contaminate their diurnal and seasonal dynamic regimes. These fluctuations and measuring errors can be removed using filtering process, for instance, centered moving average was used in this study.

The LRF and reflectors movements induced by surface and internal ice melt are able to significantly contaminate the displacement data. Appropriate technical procedures should be applied to rule out this melt effects, e.g. in-hole refreezing method used in this study and Polashenski et al. (2012). Nevertheless, careful inspection is further required to check the displacement series and to remove sudden or abnormally rapid changes. Alternatively, Helmert transformation of coordinates is necessary to screen out the impacts of possible Po movement to calculate directional strains (Prat et al. 2012).

***Comparisons with Other Results***

The recorded surface displacements of ice cover are direct evidences suggesting that the real ice strain is not equal to the thermal strain alone though thermal strain plays a dominant role. The surface displacements were detected not only at far-field sties (e.g. the present results) but also significantly at near-field sites (i.e. near dam face), even for vertical dam faces (Morse et al. 2009). All processes governing these displacements need to be investigated to simulate the static ice loads accurately. The observed residual strains $\varepsilon_R$ increased gradually with obvious daily variability. The residual strains accounted to 36% (median) or 39% (mean) of thermal strains normal to the dam while they accounted to only 7% (median) or 4% (mean) of thermal strains parallel with the dam. These values conformed that the normal stresses were consistently lower than thermal stresses while the parallel stresses close to the thermal ones (Fig. 12). This is consistent with other investigations (e.g. Morse et al. 2009, 2011).

The proposed constitutive model underlines the role of $\varepsilon_R$ in evaluating the static ice loads toward the dam face. The calculated stresses perpendicular to the dam were up to 600 kPa, favorably consistent with the near-dam stresses but much greater than the far-field stresses measured by Morse et al (2009) and Taras et al (2009). Comparisons indicated that the near-field movement is often greater than the far-field by 2~3 orders of magnitudes (Taras et al. 2009). Thus, the residual strain is likely to play a much bigger role in estimates of the near-field ice loads. With the increase in the accumulated residual strains (Fig. 10), the departure of the normal stress from the thermal stress also showed a rough trend of increase (Fig. 12). The differences of normal and thermal stresses increased from 0 kPa to 290 kPa over the observations. The parallel stresses were less than thermal stresses by 30-120 kPa before the temperature surge in phase (d) but became larger than thermal stresses during phase (d). However, since the beginning of ice formation, the ice cover endures the thermal stress and adapts itself in way of bending/buckling, cracking, creep, and ice push in response to thermal pressure and water fluctuations. The ice cover must have accumulated some residual strain prior to our observations as time goes by (like Figs. 8 and 10). Consequently, the real residual strain should be the sum of the present observed value and accumulated value prior to our investigation. Although the accumulation magnitude is not known, the real residual strain should certainly accounts for a much larger part of the thermal strain; namely, the real ice stress should be probably significantly lower than the present calculation.

Unfortunately the synchronous static stress of surface ice was not observed, so there were no direct evidences to support the present stress calculation. But a rough evaluation of the stress model performance can be done indirectly using field and tank observations at other sites (Yamaoka et al., 1988; Azarnejad and Hrudey, 1998; Morse et al., 2011; Petrich et al., 2015). The data pairs of diurnal increments in surface ice temperature $\Delta T_{diurnal}$ and the increment in ice stress $\Delta\sigma_{diurnal}$ were collected from the literatures and the present model results (Fig. 13). Generally, for a certain increase in ice temperature, the increase in ice stress was quite sparse due to varied environmental conditions and physical and mechanical properties of ice. The present model was in a good agreement with the observations in a Hokkaido reservoir by Yamaoka et al (1988), but overestimated the ice stress at other sites. Several in situ measurements of thermal ice loads/stresses were conducted in northeastern China by Sui (1988). His findings at Shengli Reservoir, which is about 80 km northeast of Hongqipao Reservoir and is quite similar to the present reservoir with respect to hydrology, meteorology, and dam structure, showed that the near-surface ice stresses were 100~400 kPa, which is very close to the present calculations.

Although the physical parameters of freshwater ice were assigned with constant values (such as $E$ and $\alpha$), these parameters are indeed temperature, strain rate and micro-texture dependent (La Placa and Post 1960; Gold 1994; Han et al. 2015). Sensitivity tests of the model indicated that the ice stress/load is significantly sensitive to the variation in elastic modulus. Therefore, accurate parameterization of elastic modulus taking into account the effects of ice temperature and strain rate is expected to make the present model more competent.

***Processes Affecting the Residual Strain***

Static ice loads on hydraulic structures have been investigated extensively for decades. Thermal deformation of ice cover induced by the ice temperature changes is the predominant driver generating the ice strains/stresses and static loads. However, many processes modify the real ice strains/stresses and loads deviating significantly from the thermal ones. These processes include water level variations (Comfort et al 2003; Stander 2006; Taras et al 2009), wet crack development (e.g. parallel fractures and block upwarping) (Carter et al 1998; Comfort et al 2003; Taras et al 2009; Comfort et al 2016), ice-boundary bonding (Comfort and Liddiard 2006; Huang et al 2017), and dry surface crack development (Fransson 1991; Azamejad and Hrudey 1998). All of these processes introduce additional strains to the thermal strain. All additional strains are included in the residual strains herein, which were measured in large scales in this study.

The water level decreased monotonously through the whole ice covered period (Fig. 2) and dropped by approximately 5 cm over our measuring duration. If we assume the reservoir ice cover is equivalent to a thin disc with edge clamped to the dam and shore since its thickness is infinitely small compared to its horizontal size. According to the bending theory of thin disc with uniform vertical loads, a 5 cm drop in water level causes an additional tensile stress of approximately 65 kPa (i.e. equivalent to a strain of $4\times10^{-5}$) to the surface of 1 m thick ice cover. This additional strain accounts for 14% of the total residual strain normal to the dam face. However, its real contribution is deemed to be much smaller than 14% because there were parallel fractures developed near and along the dam face (also in Huang et al (2017)). Parallel cracks have been frequently observed along dams and are generally located within 10 m from the dam for ice cover less than 1 m thick (Carter et al 1998; Stander 2006; Morse et al 2009). A continuous drop in water level largely makes the parallel cracks active and leads to new parallel cracks, hampering the ability of ice cover to bend.

Surface dry cracks were investigated using photography and image processing in this study although the technologies still need many more validations and evaluations. The crack density has a significant spatial variation. For instance, the crack density at 4-m scale varies from 1% to 12%. These dry cracks usually are developed due to tension, compression, and shear history. The scale dependence of spatial distribution of cracks (Fig. 9) indicates that the crack investigation should cover a spatial scale larger than a critical value (e.g. 12 m in the studied reservoir) so as to obtain a universal situation for the whole ice cover or at field scale. Spatial uncertainties are apt to grow when the scale gets smaller.

Dry cracks affect thermal ice loads in two principle ways: the expansion required to close dry cracks (especially tensile ones) delays the stress start (in other words, a part of thermal strain healing the cracks does not create ice stress), and the lateral restraint of uncracked ice decreases due to concentrated creep processes around cracks. The average crack width per confinement length (also defined as crack density) is

$$\Delta\varepsilon=\frac{\Sigma\delta_i}{L_n}, \qquad (13)$$

where $\delta_i$ is the crack width, $L_n$ is the measuring distance (Fig. 5). It is rational to assume that the ice temperature can rise up to a certain point earlier corresponding to zero pressure without creating pressure. This *free temperature rise* is correlated with the crack density and can be estimated at the surface as

$$\Delta\theta=\frac{\Delta\varepsilon}{\alpha}. \quad (14)$$

By measuring the actual free temperature rise, the crack density can be estimated from Eq. (14). The ice temperature rises during 0.5~2 h were 0.2~1.3°C, indicating the ice crack density (defined as Eq. (13)) is roughly (1~6.5)×$10^{-5}$. It is much lower than the value derived from photographing, revealing that most of cracks are closed and the crack density is somehow overestimated by the present method. This strain, if purely elastic (with $E$=1.5 GPa), would have caused a stress of 15~97.5 kPa. On the other hand, ice cracks, opening and closed, decrease the contact area between uncracked ice, thus, decrease the lateral confinement. This reduction was expressed as a reduction in modulus, which was found to be a function of crack depth and the distance between two neighboring cracks (Fransson 1991). Ice creep is believed to be accelerated within regions surrounding the cracks (Sinha 1988). However, little is known on the elastic, viscous, and creep behaviors of cracked ice under compressive and shear loads, calling for a great number of experimental and theoretical efforts.

Wind drag also creates ice stresses and loads on dams. Surface drag coefficient is assumed to be 1.5×$10^{-3}$ (Prinsenberg and Petersen 2002), a strong wind with speed of 10 m/s causes a shear stress of 0.2 Pa to the surface ice. For a fetch of 10 km (normal to the main dam line), the wind stress integrates to a line force of 2 kN/m on the dam face. These values are negligibly small compared with the residual stress and calculated normal stress. However, the irregular shape of reservoir is expected to lead to a significant spatial variation in wind-induced line load on dam face especially around sharp corners.

Furthermore, some artificial activities (e.g. ice trench excavating in Ma and Li (2011)) and nearshore terrain (bathymetry) also influence the ice displacement, strain, and stress (Stander 2006). In order to better understand these processes and their impacts on ice loads, many more field efforts are still called for to gain experiences, especially on the impacts of the development and dynamics of dry and wet cracks, ice edge bonding situations, and creep behaviors of freshwater ice under cyclic loads.

## Conclusion

With the help of a robust laser range finder, a reservoir ice cover was monitored for displacements in the presence of incompletely confined boundaries, ice crack development, and water level drops, in response to thermal pressure. The recorded displacements of surface ice indicated that the real ice strain deviates significantly from the thermal strain. Residual strains were introduced and calculated from the displacement datasets. The residual strain is scale-dependent when the measured range is less than about 12 m at this reservoir due to spatial variation of crack development. It shows a similar diurnal and seasonal variation with air/ice temperature, but its daily amplitude is usually lower than the thermal strain. The water level fluctuations, parallel crack dynamics, surface (dry) cracks development, and reservoir geometry have universal or site-specific impacts on residual strains.

The ice strain should consist of thermal strain and residual strain rather than the former alone used previously to estimate the ice stress. Both the ice strain and residual strain are anisotropic largely due to the boundary shape. Although the principle strain and strain normal to and parallel with the dam have similar trends with the thermal strain, the first principle and parallel strains are quite close to the thermal strain except during a sharp increase in ice temperature and the principle direction is roughly towards the reservoir center in spite of early fluctuations. The normal strain is always lower than the thermal strain possibly due to strain release by the ice dynamics on the dam face, parallel fractures, upheavals of cracked ice blocks, dry crack development, and ice creep (Carter et al., 1998; Ma and Li, 2011).

A new constitutive model was developed to take into account the residual strain. Using the observed residual strain, both principal and normal stresses (i.e. perpendicular to the dam) were estimated. The predicted normal stress is in an acceptable agreement with field measurements through indirect comparisons. The present model indicated that the residual strain/surface deformation has a significant impact on the surface ice stress. The residual strain could release 39% (with a maximum of 65%) of the thermal stress normal to the dam and only 7% parallel with the dam during the observing period, indicating that the residual strain is the key reason for the ice load overestimation of previous models. In this context one may wish to discriminate the impacts of ice boundary dynamics, crack development, and water level fluctuation on the residual strain. This is important and challenging so as to model the residual strain, and requires many more field experiences and theoretical work.

## Acknowledgments

This research was supported by the National Natural Science Foundation of China (No. 41402203 and 51579028) and the Special Fund for Basic Scientific Research of Central Colleges (310829171002). We are also grateful to Dr. Yu Yang from Shenyang Institute of Engineering, Mr. Yanfeng Cheng from Polar Research Institute of China, and the staff from the Executive Department of Hongqipao Reservoir for their field assistance and theoretical discussion.

## References

Arunachalam, A.V.M. (2005). "Application of dimensional analysis to estimation of ice-induced pressures on rigid vertical structures." *Can. J. Civil Eng.*, 32, 968-980.

Azarnejad, A., and Hrudey, T.M. (1998). "A numerical study of thermal ice loads on structures." *Can. J. Civil Eng.*, 25, 557-568.

Bergdahl, L. (1978). "Thermal ice pressure in lake ice covers." *Report Series A:2*, Depart. Hydraul., Chalmers Univ. Technol., Goteborg, Sweden (164 pp).

Bouaanani, N., Paultre P., and Proulx J. (2004). "Dynamic response of a concrete dam impounding an ice-covered reservoir: Part I. Mathematical modelling." *Can. J. Civil Eng.*, 31(6), 956-964.

Boulton, G.S., and Jones, A.S. (1979). "Stability of temperate ice caps and ice sheets resting on beds of deformable sediments." *J. Glaciol.*, 24(90), 29-43.

Carter, D., Sodhi, D., Stander, E., Caron, O., and Quach, T. (1998). "Ice thrust in reservoirs." *J. Cold Reg. Eng.*, 12(4), 169-183.

Comfort, G., Côté, A., and Taras, A. (2016). "Processes and limits controlling ice loads on dams." *Proc. 23rd IAHR Int. Symp. on Ice*, Ann Arbor, Michigan, USA.

Comfort, G., Gong, Y., and Singh, S. (2000a). "Static ice loads for dam safety analysis." *Proc. 3rd Can. Dam Safety Conf.*, Regina, Saskatchewan, Canada.

Comfort, G., Gong, Y., Singh, S., and Abdelnour, R. (2000b). "Predicting static ice loads on dams." *Proc. 15th IAHR Int. Symp. on Ice*, Gdansk, Poland, 135-143.

Comfort, G., Gong, Y., and Singh, S. (2000c). "The factors controlling static ice loads on dams." *Proc. 15th IAHR*

*Int. Symp. on Ice*, Gdansk, Poland, 189-197.

Comfort, G., Gong, Y., Singh, S., and Abdelnour, R. (2003). “Static ice loads on dams.” *Can. J. Civil Eng.*, 30(1), 42-68.

Comfort, G., and Liddiard, A. (2006). “Ice-induced damage to shoreline properties on Round and Golden lakes.” *Proc. 18th IAHR Int. Symp. on Ice*, Sapporo, Japan, 21-28.

Cox, G.F.N. (1984). “A preliminary investigation of thermal ice pressures.” *Cold Reg. Sci. Technol.*, 9(3), 221-229.

Fransson, L. (1988). “Thermal ice pressure on structures in ice covers.” *Ph.D. Thesis*, Luleå Univ. Technol., Luleå, Sweden.

Fransson, L. (1991). “Do cracks reduce thermal ice stresses?” In: Jones, S., Tillotson, J., Makenna, R. F., Jordaan, I. J. (eds) *Ice-Structure Interaction*, International Union of Theoretical and Applied Mechanics (International Association for Hydraulic Research). Springer, Berlin, Germany.

Gebre, S., Alfredsen, K., Lia, L., Stickler, M., and Tesaker, E. (2013). “Review of ice effects on hydropower systems.” *J. Cold Reg. Eng.*, 27(4), 196-222.

Gold, L.W. (1994). “The elastic modulus of columnar-grain fresh-water ice.” *Ann. Glaciol.*, 19(2), 13-18.

Han, H., Jia, Q., Huang, W., and Li, Z. (2015). “Flexural strength and effective modulus of large columnar-grained freshwater ice.” *J. Cold Reg. Eng.*, doi: 10.1061/(ASCE)CR.1943-5495.0000098.

Huang, W., Li, Z., Han, H., and Jia, Q. (2017). “Limit resistive forces from ice frozen to concrete-revetment interface of an inclined dam wall.” Cold Reg. Sci. Technol., 141, 181-187.

Huang, W., Lu, P., Lei, R., Xie, H., and Li, Z. (2016). “Melt pond distribution and geometry in high Arctic sea ice derived from aerial investigations.” *Ann.Glaciol.*, 57(73), 105-118.

Ivchenko, A.B. (1990). “Investigation of stress of ice cover under changes of temperature.” *Proc. IAHR 10th Symp. on Ice*, Espoo, Finland, 149-157.

Jia, Q. (2012). “Study on design ice parameters of slope protection on plain reservoir in cold regions.” *Doctoral Dissertation*, Dalian University of Technology, Dalian, China. (in Chinese with English abstract)

Jia, Q., Li, Z., and Leppäranta, M. (2010). “Estimation of annual maximum ice thickness in different return periods for a reservoir using air temperature.” *Proc. 20th IAHR Int. Symp. on Ice*, Lahti, Finland.

Kharik, E., Morse, B., Roubtsova, V., Fafard, M., Côté, A., and Comfort, G. (2017). “Numerical studies for a better understanding of static ice loads on dams.” *Can. J. Civil Eng.*, doi: 10.1139/cjce-2017-0142.

Kharik, E., Roubtsove, V., Morse, B., Fafard, M., Côté, A., and Taras, A. (2015). “Impact of ice type on predicted ice load for dams." *Proc 18th CRIPE Workshop on River Ice*. CGU HS Committee on River Ice Processes and the Environment, Quebec City, QC, Canada.

Ko, P.K., Ho, M.S., and Smith, G..F. (1994). "Thermal ice forces on concrete dams recent development." *Proc. 1994 Can. Dam Safety Conf.*, Winnipeg, Manitoba, Canada, 17-33.

La Placa, S.J., and Post, B. (1960). "Thermal expansion of ice." *Acta Cryst.*, 13(6), 503-505.

Ma, H., and Li, F. (2011). "A mechanism study on restricting static ice pressure by excavating trench method." *Cold Reg. Sci. Technol.*, 66, 39-43.

Morse, B., Stander, E., Côté, A., Morse, J., Beaulieu, P., Taras, A., Noël, P., and Pratt, Y. (2009). "Ice interactions at a dam face." *Proc 15th CRIPE Workshop on River Ice*. CGU HS Committee on River Ice Processes and the Environment, St. John's, Newfoundland and Labrador.

Morse, B., Stander, E., Côté, A., Richard, M., and Desmet, V. (2011). "Stress and strain dynamics in a hydroelectric reservoir ice sheet." *Proc. 16th Workshop on River Ice*, CGU HS Committee on River Ice Processes and the Environment, Winnipeg, Manitoba, Canada. 303-316.

Petrich, C., Sæther, I., Fransson, L., Sand, B., and Arntsen, B. (2015). "Time-dependent spatial distribution of thermal stresses in the ice cover of a small reservoir." *Cold Reg. Sci. Technol.*, 120, 35-44.

Polashenski, C., Perovich, D., and Courville, Z. (2012). "The mechanisms of sea ice melt pond formation and evolution." *J. Geophys. Res.*, 117, C01001, doi: 10.1029/2011JC007231.

Prat, Y., Desmet, V., Santerre, R., Morse, B., and Bourgon, S. (2012). "Continuous monitoring of an ice sheet in a reservoir upstream of Beaumont Dam, Canada." *J. Surv. Eng.*, 138(1), 37-45.

Prinsenberg, S.J., Fowler, G.A., van der Baaren, A., and Beanlands, B. (1997). "Ice stress measurements from land-fast ice along Canada's Labrador Coast." *Cold Reg. Sc. Technol.*, 25, 1-15.

Prinsenberg, S., and Peterson I.K. (2002). "Variations in air-ice drag coefficient due to ice surface roughness." *Int. J. Offshore Polar Eng.*, 12(2), 121-125.

Sinha, N. K. (1988). "Crack-enhanced creep in polycrystalline material: strain-rate sensitive strength and deformation of ice." *J. Mater. Sci.*, 23, 4415-4428.

Stander, E. (2006). "Ice stresses in reservoirs: effect of water level fluctuations." *J. Cold Reg. Eng.*, 20(2), 52-67.

Sui, X. (1988). "Study on ice static pressure on ice cover in reservoir." *Proc. 9th IAHR Symp.on Ice*, Sapporo, Japan, vol. 1, pp. 483-493.

Taras, A., Côté, A., Morse, B., Stander, E., Comfort, G., Noël, P., Pratt, Y., and Lupien, R. (2009). "Measurement of ice thrust on dams." *Proc. CDA 2009 Ann. Conf.*, Whistler, British-Columbia, Canada.

Timco, G. W., Watson, D. A., Comfort, G., and Abdelnour, R. (1996). "A comparison of methods for predicting thermally-induced ice loads." *Proc. IAHR Ice Symp.*, Beijing China, 241-248.

Xu, B. (1986). "Design value of pressure due to expansion of ice sheet in reservoir." *Proc. 8th IAHR Symp. on Ice*, Iowa City, US, Vol. 1, 231-238.

Yamaoka, I., Fujita, M., and Hasegawa, K. (1988). "Measurement of thermal ice thrust exerted by an expanding ice cover in Taisetsu Dam Reservoir in Hokkaido, Japan." *Proc. 9th IAHR Symp. on Ice*, Sapporo, Japan, Vol. 1, 473-482.

Zhang, L., Li, Z., Jia Q., and Huang, W. (2012). "Experimental study on uniaxial compressive strength of reservoir ice." *Trans. Tianjin Univ.*, 18(2), 112-116.

**Table 1.** Parameters and coefficients of freshwater reservoir ice for the stress model

| Name | Symbol | Value |
| --- | --- | --- |
| Elastic Modulus | $E$ | 1.5 GPa (Zhang et al. 2012; Han et al. 2015) |
| Expansion coefficient | $\alpha$ | $5.0\times10^{-5}$/°C |
| Viscous creep rate | $K$ | $KD=\beta\cdot(\frac{T_*}{T})^m$, where $\beta=2.46\times10^{-29}$/s, $T_*=-1$°C, $m=1.92$ (Cox 1984; Petrich et al. 2015) |
| Coefficient of viscous deformation | $D$ | |
| Coefficient | $n$ | 3.7 (Petrich et al. 2015) |
| Reference stress | $\sigma_0$ | 100 kPa |
| Time step | $h$ | 1800 s |
| Initial stress | $\sigma_{(0)}$ | 10 kPa |

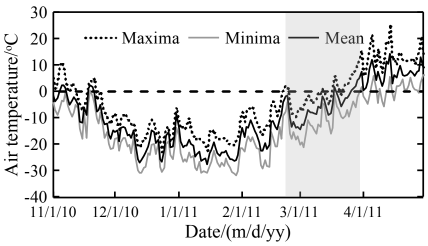


**Fig. 1.** Daily air temperature during winter 2010-11 from Anda meteorological station. The time series is in good agreement with our field data (Jia et al. 2010). The field experiment period is highlighted grey.

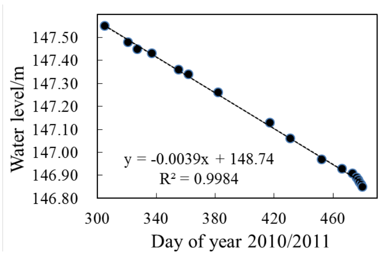


**Fig. 2.** Water level variation in Hongqipao reservoir during the ice season 2010-2011 (Day 305 denotes Nov. 1, 2010).

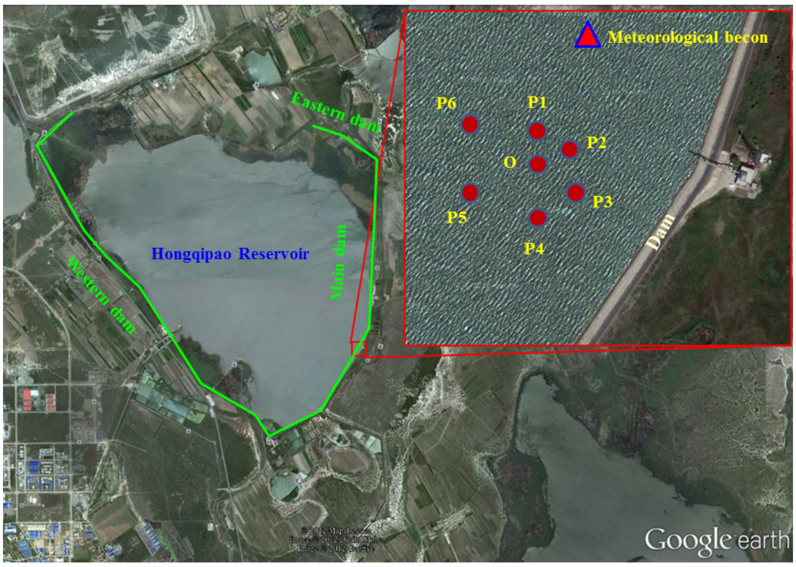


**Fig. 3.** The location of Hongqipao reservoir and the layout of instrumentation site (Google Earth).

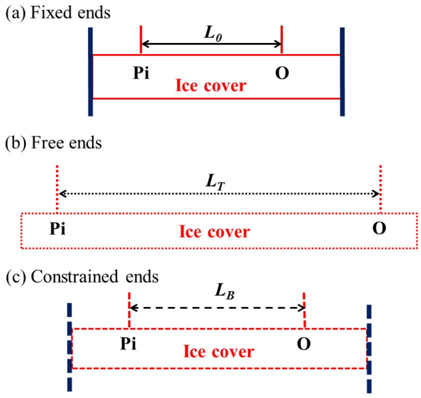


**Fig. 4.** Ice cover displacement within different confined boundaries. Points O and Pi denote the positions of LRF and reflector, respectively. $L_0$, $L_T$, and $L_B$ denote the distances between O and Pi after a temperature increase for fixed (a), free (b), and incompletely constrained (c) ends, respectively.

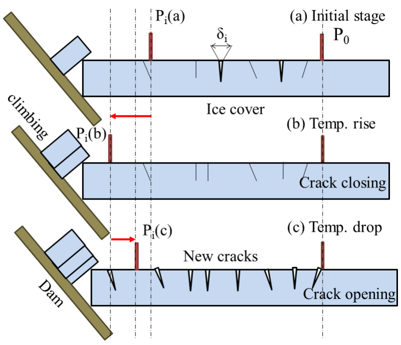


**Fig. 5.** The ice edge dynamics on the dam face and the development of cracks.

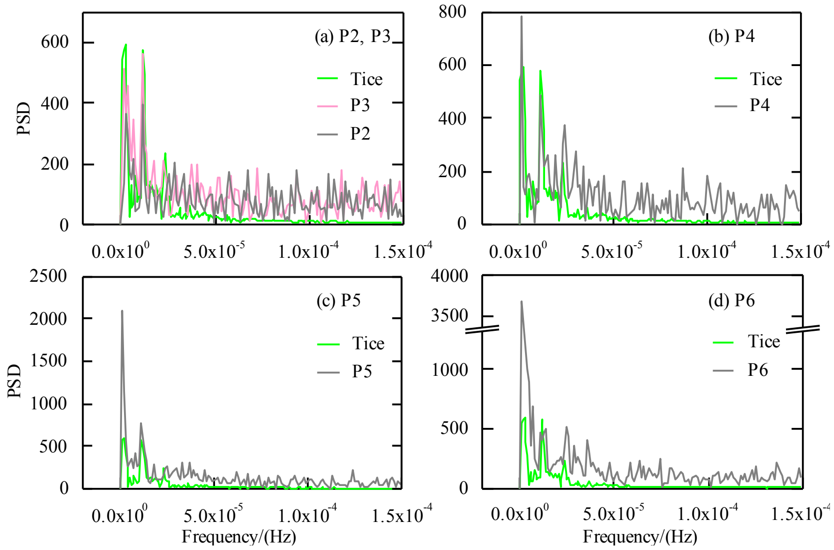


**Fig. 6.** Power spectrums for directional displacements and ice temperature. PSD is short for power spectral density.

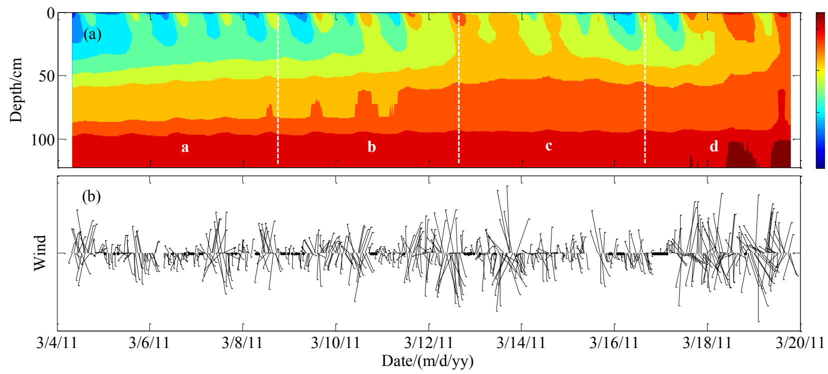


**Fig. 7.** Ice temperature (a) and wind series (b) during the campaign, divided into four phases (a-d). The depth was below ice surface (0 cm). Data at 102 and 122 cm depths show actually temperatures of water under ice.

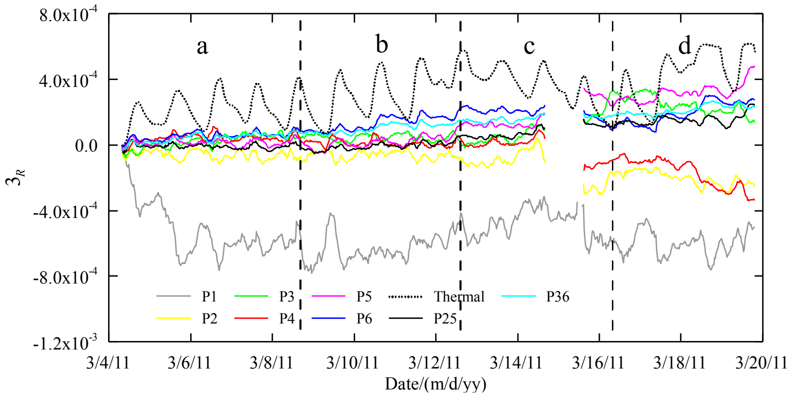


**Fig. 8.** The observed residual strain $\varepsilon_R$ and thermal strain $\varepsilon_T$ from March 4 to 20 in 2011.

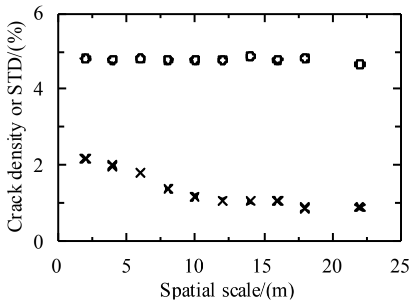


**Fig. 9.** The crack density (○) and its standard deviation (STD, ×) at different spatial scale over the ice cover surface.

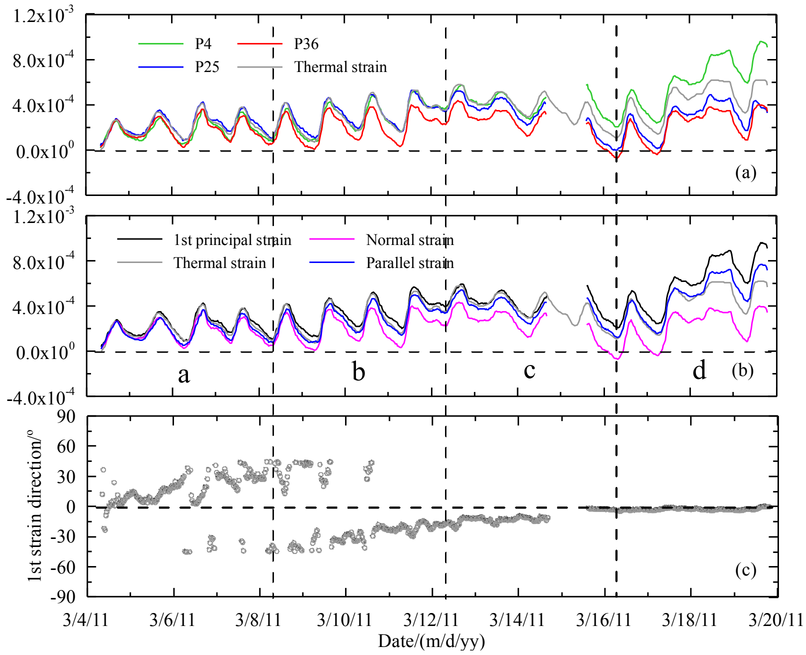


**Fig. 10**. The first principal strain (*b*) and its direction (*c*) derived from lines 4 (green), 2-5 (blue) and 3-6 (red) as well as thermal strain (grey) (*a*). The direction of the first principal strain is positive counterclockwise with the zero pointing to the north. The normal and parallel strain

denotes the strain perpendicular to and parallel with the nearby dam face, the azimuth of which is roughly -30°.

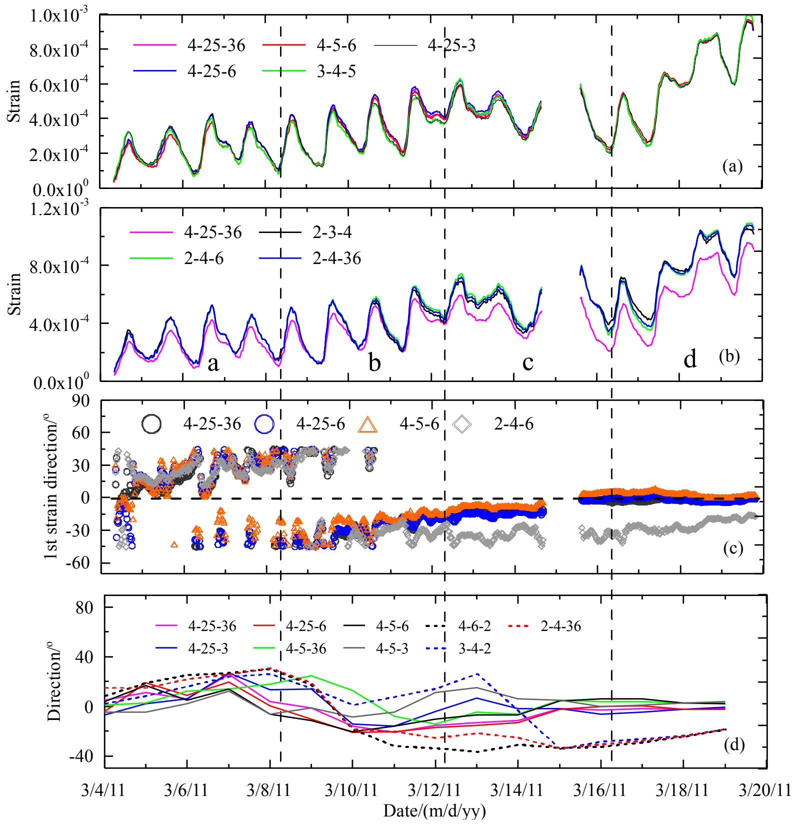


Fig. 11. Values (*a*, *b*), directions (*c*), and daily averages of directions (*d*) of the first principle strains calculated from different triangles of directional strains.

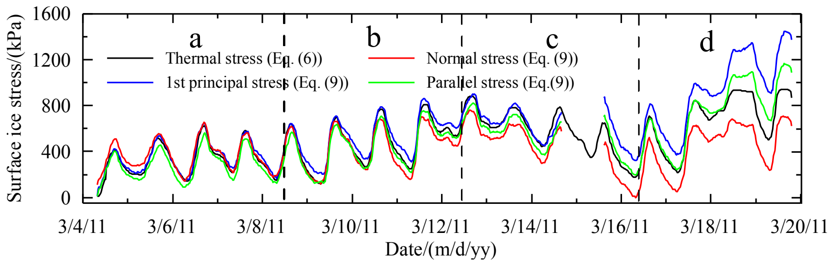


**Fig. 12.** The surface ice stresses derived from strains. The normal and parallel stresses are perpendicular to and parallel with the nearby dam face, respectively.

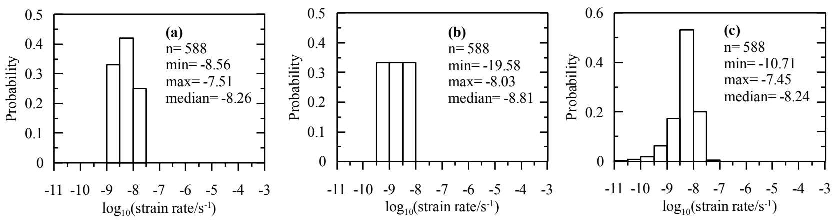


**Fig. 13.** The strain rate distribution of the thermal strain (*a*), residual strain of P36 (*b*) and principle strain (*c*) of surface ice.

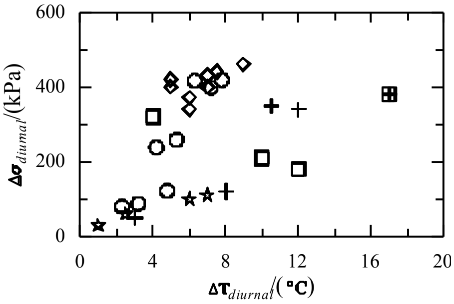


**Fig. 14.** The relationships of the diurnal increments in ice temperature $\Delta T_{diurnal}$ vs stress $\Delta\sigma_{diurnal}$ derived from the present stress model results (circle), and from field and experiment results by Azarnejad and Hrudey (1998) (square), Morse et al (2011) (cross), Petrich et al (2015) (star), and Yamaoka et al (1988) (diamond).